

# Super-Heating and Micro-Bubble Generation around Plasmonic Nanoparticles under cw Illumination

Guillaume Baffou,<sup>\*,†</sup> Julien Polleux,<sup>‡,§</sup> Hervé Rigneault,<sup>†</sup> and Serge Monneret<sup>†</sup>

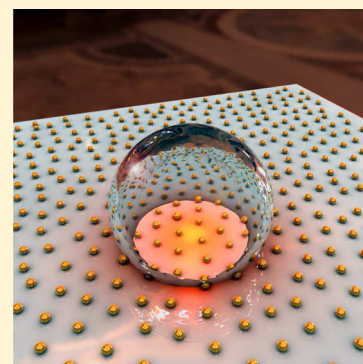
<sup>†</sup>Institut Fresnel, CNRS, Aix Marseille Université, Centrale Marseille, UMR 7249, 13013 Marseille, France

<sup>‡</sup>Max Planck Institute of Biochemistry, Department of Molecular Medicine, 82152 Martinsried, Germany

<sup>§</sup>Center for NanoScience, Ludwig Maximilian University, 80799 Munich, Germany

## S Supporting Information

**ABSTRACT:** Under illumination, metal nanoparticles can turn into ideal nanosources of heat due to enhanced light absorption at the plasmonic resonance wavelength. In this article, we aim at providing a comprehensive description of the generation of microbubbles in a liquid occurring around plasmonic nanoparticles under continuous illumination. We focus on a common situation where the nanoparticles are located on a solid substrate and immersed in water. Experimentally, we evidenced a series of singular phenomena: (i) the bubble lifetime after heating can reach several minutes, (ii) the bubbles are not made of water steam but of air, and (iii) the local temperature required to trigger bubble generation is much larger than 100 °C: This last observation evidences that superheated liquid water, up to 220 °C, is easy to achieve in plasmonics, under ambient pressure conditions and even over arbitrary large areas. This could lead to new chemical synthesis approaches in solvothermal chemistry.



## INTRODUCTION

Noble metal nanoparticles can turn into ideal nanosources of heat when illuminated at their plasmonic resonance wavelength. The field of research based on this simple concept is named thermoplasmonics<sup>1</sup> and has already led to valuable applications, especially in biology and medicine, such as photothermal cancer therapy,<sup>2</sup> photothermal imaging,<sup>3</sup> drug and gene delivery,<sup>4,5</sup> and photoacoustic imaging.<sup>6,7</sup> More recently, this field of research led to more fundamental developments in areas such as nanochemistry,<sup>8</sup> thermal biology at the single cell level,<sup>9</sup> or plasmofluidics.<sup>10–12</sup>

Photothermal bubble generation induced around plasmonic nanoparticles is a thermoplasmonic process that has been studied during the past decade mainly under *pulsed* illumination and in the context of biorelated applications. The large amount of energy of a femtosecond laser pulse can generate a strong, brief, and confined temperature increase around illuminated plasmonic nanoparticles,<sup>13</sup> eventually followed by a short-lived bubble nucleation.<sup>14–16</sup> This effect can lead to a local destruction of biological tissues or membranes for applications in nanosurgery<sup>17,18</sup> or trigger the propagation of a shock wave for applications in photoacoustic imaging.<sup>6,7,19</sup>

A more recent and less investigated related field of research concerns the photothermal bubble generation in plasmonics under *continuous wave* (cw) illumination. In 2011, Hühn et al.<sup>20</sup> were the first to study bubble generation around nanoparticles under cw heating and to hypothesize superheating. In 2012, Neumann et al.<sup>21</sup> reported on the generation of nanobubbles from gold nanoparticles under solar illumination, i.e., weaker light intensity in comparison to experiments based on laser

illumination. The authors envisioned applications in waste or surgical instruments sterilization in the third world. In 2013, the same group published a close related work intended to theoretically describe the bubble generation around metal nanoparticles under illumination, based on simple thermodynamics considerations.<sup>22</sup> Even more recently, Zhao et al. proposed a first application of plasmon-induced microbubbles (MBs) that consists of generating a surface MB on a metal film as an effective lens for surface plasmon waves in a microfluidic environment.<sup>10</sup> However, despite these few recent breakthroughs in plasmonics, the nature of plasmon-induced MBs remains not clarified, and associated physical processes not exhaustively described. In particular, the role of dissolved air molecules in the liquid is usually not identified, although it plays a fundamental role in the bubble dynamics. Moreover, the question of the actual temperature increase required to generate a MB is not addressed.

In this article, we aim at providing a comprehensive description of the physics of MBs created by plasmonic nanoparticles heated under cw illumination and immersed in a liquid. First, we focus on the physics of the MB *generation*. The nature of the bubble is explained, along with the influence of the presence of dissolved air molecules in the liquid. We also evidence a temperature threshold prior bubble formation that substantially exceeds 100 °C, the boiling point of water under ambient conditions, independently of the size of the heated

**Received:** November 22, 2013

**Revised:** January 6, 2014

**Published:** January 8, 2014

nanoparticle array. Then, we describe the *shrinkage* of MBs at ambient temperature and explain their unexpected long lifetime measured experimentally. A final part is dedicated to describe the MB steady state maintained under illumination.

## EXPERIMENTAL METHOD

**Sample Description.** The substrate consists of a uniform quasi-hexagonal array of spherical gold nanoparticles on a glass coverslip (Figure 1a). The sample was made by diblock

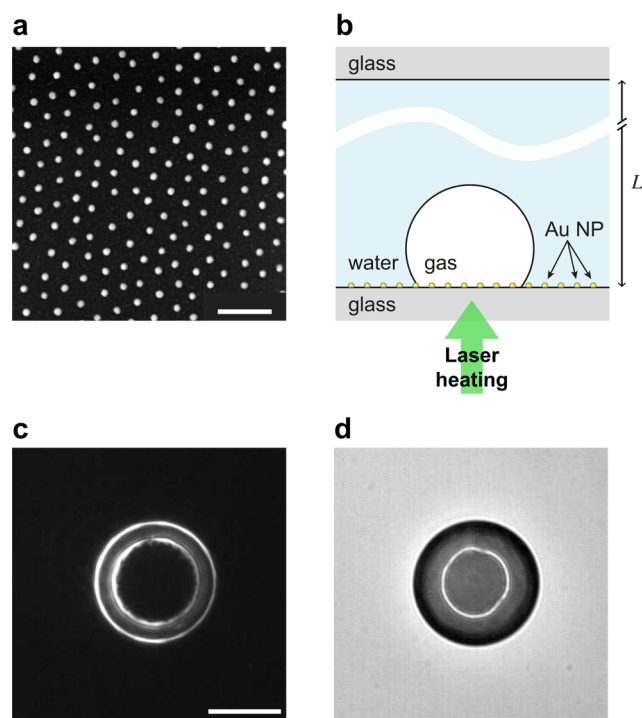


**Figure 1.** (a) Scanning electron microscope (SEM) image of a substrate covered with a uniform quasi-hexagonal array of gold nanoparticles (scale bar: 200 nm). (b) Schematic of the system that consists of a microbubble on the substrate immersed in water. The bubble is generated by heating the gold nanoparticles with laser illumination. (c) Dark field imaging of a single microbubble (scale bar: 20  $\mu\text{m}$ ). (d) Bright field imaging of the same microbubble.

copolymer micellar lithography.<sup>23</sup> The nanoparticles were typically 28 nm in diameter and featured an interparticle distance of 72 nm in average. A drop of water was deposited on top of the sample and then covered with another coverslip to obtain a 1 mm thick water layer. A full description of the sample geometry is provided in the Supporting Information. In such a configuration, the plasmonic resonance of the nanoparticle assembly is located around 530 nm. When such a system is locally illuminated at this wavelength, efficient light absorption occurs at the glass–water interface, where the nanoparticles are located, which generates a temperature increase in the surrounding water.<sup>1</sup> If the light intensity is strong enough, a MB generation occurs at the interface, as sketched in Figure 1b.

The advantage of such a sample is that the NP distribution is regular and perfectly uniform over a centimetric area on the coverslip. This way, for a given laser beam diameter and power, the temperature increase is the same irrespectively of the location of the laser beam on the sample. Besides the uniformity of the NP distribution, the other advantage is the

small NP interdistance. Indeed, when heating dense arrays of NPs, the temperature increase is no longer spatially localized around each NP. On the contrary, the temperature distribution is smooth throughout the set of illuminated NPs due to collective thermal effects, as we explained in a recent publication.<sup>24</sup>

**Set-up Description.** The optical setup used to generate plasmon-induced MBs and perform the optical and thermal measurements is depicted in Figure 2. In order to generate heat,

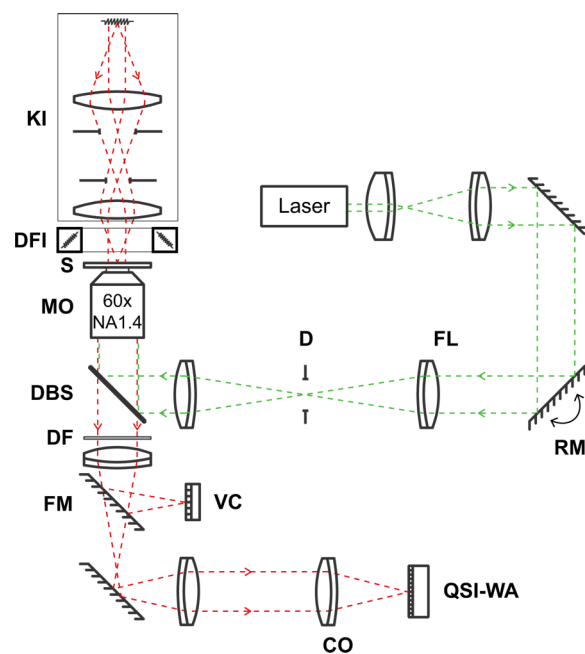


**Figure 2.** Schematic of the optical setup used to photothermally generate the bubbles and perform the optical and thermal measurements. KI, Köhler illumination; DFI, dark field imaging; S, sample; DBS, dichroic beam splitter; DF, dichroic filter; FM, flip mirror; VC, video camera; CO, camera objective; QSI-WA, wavefront analyzer based on quadriwave shearing interferometry; D, diaphragm; FL, flip lens; RM, rotating mirror.

the nanoparticle array is illuminated from the bottom through the microscope objective (MO) (Olympus 100 $\times$ , oil, 1.3 NA and Olympus 40 $\times$ , oil, 1.35 NA) using a laser illumination at a wavelength of 532 nm. Two illumination conditions can be applied: (i) A focused illumination to heat a sub-micrometric diffraction-limited area. In this first case, which is the one represented in Figure 2, the focalization spot of the laser illumination on the sample can be displaced by manually rotating the mirror RM. (ii) A circular wide-field illumination (WFI) obtained by removing the flip lens FL in order to focus the laser at the entrance pupil of the objective MO. In this second case, the beam diameter at the sample location is adjusted using the diaphragm D. The video camera VC is used to take images and videos of the MBs either under standard Köhler illumination (KI) or dark field illumination (DFI). In order to map the temperature, a TIQSI (temperature imaging using quadriwave shearing interferometry) configuration was implemented.<sup>25</sup> It consists of a KI and a Sid4Bio wavefront analyzer<sup>26</sup> (based on quadriwave lateral shearing interferometry) QSI-WA.

Here is in brief the principle of the TIQSI technique: When the temperature  $T$  increases, the liquid features a modification of its refractive index  $n$ , which creates a distortion of the KI

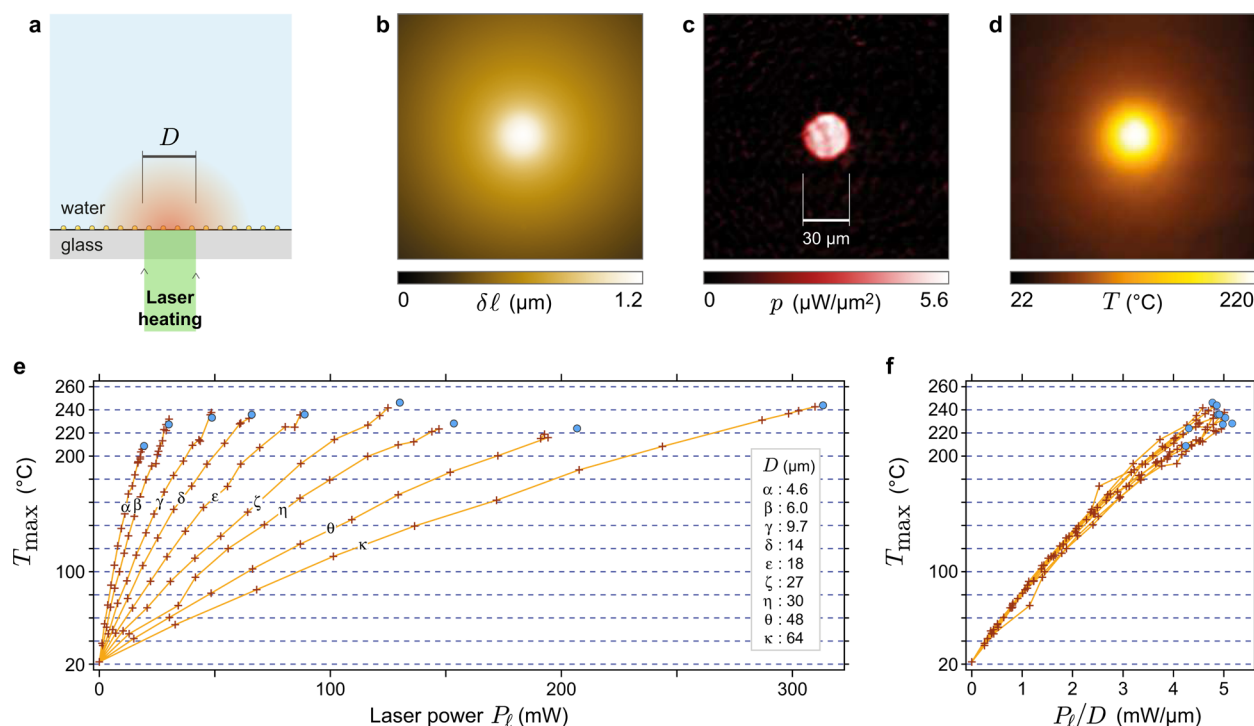


**Figure 3.** (a) Schematic of the experiment. (b) Thermal-induced optical path difference measured by TIQSI. (c) Heat source density retrieved from image a, which naturally matches the laser beam shape. (d) Temperature map retrieved from image c, featuring a maximum temperature of  $T_{\max} = 220$  °C. (e)  $T_{\max}$  as a function of the laser power  $P_l$  for a set of various beam diameters  $D$ . The occurrence of a bubble formation for each curve is spotted by a blue disc. (f)  $T_{\max}$  as a function of the ratio  $P_l/D$  for the same set of various beam diameters  $D$ , featuring an expected invariant profile.

planar wavefront, subsequently measured by the wavefront analyzer. The temperature distribution in the sample is then retrieved from this wavefront distortion using an inversion algorithm, based on the knowledge of the function  $\beta(T) = dn/dT$  (see the Supporting Information and ref 27). Even though the temperature distribution could be retrieved in three dimensions using the TIQSI technique,<sup>28</sup> all the temperature maps presented herein represent the temperature distribution at the glass–liquid interface, i.e., where the nanoparticles are located. Since this optical technique is diffraction limited, the measured temperature is actually an average temperature over a diffraction limited volume that is less than 1  $\mu\text{m}$  in size. In our configuration, since the heated area is always larger than a few micrometers, spatial variations of the temperature distribution are supposed to be smooth at the micrometer scale, even along the  $z$  axis.<sup>28</sup> Hence, the temperature is not supposed to be underestimated due to any spatial under-sampling.

Note that temperature measurements are possible only prior to MB formation. Indeed, once a MB appears, the optical wavefront is not only distorted by the thermal-induced refractive index variation of the water layer but also by the MB itself. This restriction was not a limitation within the scope of this work.

## RESULTS AND DISCUSSION

**Bubble Formation.** To begin with, we will focus on the nature of the MB generated from plasmonic nanoparticles in water. Such bubbles, generated by heterogeneous nucleation, are not supposed to be made of water steam but rather of air molecules. In practice, there are always air molecules adsorbed on solid surfaces<sup>29,30</sup> and there is also always a large amount of air molecules dissolved in water, unless it was previously degassed. The MBs observed in plasmonics experiments

originate from these dissolved air molecules. In 2013, Deguchi et al. studied the formation of MBs on a carbon microfiber.<sup>31</sup> The authors explained that, when generating MBs from a micrometric source of heat in water, water vaporization was responsible for the primary formation of the bubbles, and their subsequent expansion was caused by the diffusion of dissolved gases. In other words, as soon as a MB appears, if a dissolved gas is present in the liquid (say  $\text{N}_2$ , for instance), a  $\text{N}_2$  diffusion occurs in the liquid and across the MB boundary to fill in the MB until an equilibrium between the chemical potentials of  $\text{N}_2$  inside and outside the MB is achieved. At equilibrium, one has the Henry law:

$$P = Kc \quad (1)$$

where  $P$  is the partial pressure of  $\text{N}_2$  in the MB,  $K$  is the Henry coefficient, and  $c$  is the  $\text{N}_2$  concentration in the liquid just at the MB boundary. The fact that the MBs are mainly made of air molecules is also evidenced by their long lifetimes. Once formed, and upon stopping the laser heating, a MB can last from a few seconds to several hours, depending on its initial size. If the MBs were made of water steam, they would disappear as soon as the heating is stopped. The shrinkage of the MBs is discussed in detail in the next section.

Another interesting feature is the actual temperature value  $T_B$  required to generate a MB, which was observed to be much larger than 100 °C, the water boiling temperature under 1 atm. Experimental results are gathered in Figure 3. The experiment consisted of illuminating an area of diameter  $D$  for 5 s (Figure 3a) and measuring the temperature distribution meanwhile. This procedure was repeated for various laser powers, from low to high, until a MB appeared, in order to estimate the temperature threshold  $T_B$  of MB formation, and figure out whether  $T_B$  is dependent on the size of the heated area. Parts

b–d of Figure 3 present a thermal imaging measurement using the TIQSI technique where the laser power was set just below the power threshold required to trigger the generation of a bubble. In this example, the water temperature reaches a maximum of  $T_{\max} \approx 220$  °C at the laser spot location. All the measurements are gathered in Figure 3e for beam diameters  $D$  ranging from 4.6 to 64  $\mu\text{m}$ . The occurrence of MB formations is spotted using blue discs. Interestingly,  $T_{\text{B}}$  turns out to be rather independent of the size of the heated area. Regardless of the size of the heated area, a bubble formation systematically occurred between 220 and 240 °C. Figure 3e evidences that a small laser diameter requires a much smaller laser power to generate a bubble. Hence, the occurrence of a bubble formation cannot be determined by simply considering the power  $P_l$  sent on the sample. It is also not a function of solely the laser intensity  $P_l/D^2$  (power per unit area). The occurrence of a MB is determined solely by the quantity  $P_l/D$ . This trend comes from the fact that the source of heat is *two-dimensional*. Indeed, when illuminating a two-dimensional uniform distribution of nanoparticles, the temperature achieved in the medium is proportional to  $P_l/D$ , as we recently detailed in ref 24. To illustrate this effect, Figure 3f displays the results presented in Figure 3e as a function of  $P_l/D$  and an overlap is observed between line shapes, as expected.

The reason for this particular temperature threshold at around 230 °C is not understood for the time being. This temperature is not a significant temperature for water: It is neither the boiling temperature at ambient pressure (100 °C) nor the spinodal decomposition temperature of water (around 320 °C). We do not exclude possible systematic error in the temperature estimation using the TISQI technique at such high temperatures. Indeed, the retrieval of the temperature from the wavefront distortion is based on solely the knowledge of the refractive index of water as a function of the temperature over the temperature range investigated. For this, we trust what was reported in ref 27. Then, estimating the temperature using the TIQSI technique does not require the knowledge of the thermal conductivity of water. However, a dependence of the thermal conductivity of water as a function of temperature may induce some systematic error, but the thermal conductivity of water is not strongly dependent on temperature (less than 10% variation over the temperature range investigated).

The occurrence of a liquid heated above its boiling point and being in a metastable state is a phenomenon known as *superheating*. This phenomenon is well-known, and the absence of bubble formation can be explained by classical nucleation theory:<sup>32</sup> A bubble is characterized by an inner pressure that reads

$$P_{\text{MB}} = P_{\infty} + \frac{2\gamma}{a} \quad (2)$$

where  $\gamma$  is the surface tension of the liquid,  $P_{\infty}$  the ambient pressure, and  $a$  the radius of the MB. For instance, in water under atmospheric pressure, a bubble of 1  $\mu\text{m}$  in diameter features an inner pressure of 3.4 bar ( $\gamma \approx 0.059$  N·m<sup>-1</sup> at 100 °C). At such a pressure, the boiling point is larger than 100 °C. The formation of a micrometric bubble at 100 °C would thus lead to a paradox: water steam at 100 °C under a few bars. The direct consequence is that no liquid–gas interface appears at 100 °C. However, this effect does not explain by itself a superheating up to 220 °C. Indeed, the boiling temperature under a few bars does not exceed 150 °C. There is another

effect that will further prevent the formation of a MB: Even if a MB would be thermodynamically stable, an energy barrier still remains to be overpassed to generate a MB.<sup>32</sup> This energy reads

$$\Delta E = 4\pi a^2 \gamma \quad (3)$$

The formation of a MB is thus governed by the Arrhenius law. Bubble formation (boiling) occurs only when this energy barrier is crossed, one way or another.

In everyday life, boiling is yet observed systematically around 100 °C, despite the few considerations above. The reason is that most surfaces are endowed with nucleation centers that contribute to lowering the energy barrier  $\Delta E$ .<sup>20</sup> Nucleation centers can be impurities or surface scratches. In the present work, we used glass coverslips, which are particularly clean and flat, avoiding the presence of nucleation centers. This is the origin of the systematic superheating observed in our experiments. As an example, in chemistry, since glassware surfaces are also usually perfectly flat and cleaned, superheating may occur in some experiments, even at the macroscale. This is why a pumice stone is often added to a reaction medium as an efficient provider of nucleation centers, in order to avoid superheating and subsequent hazardous explosive boiling.

Although superheating is a phenomenon discovered a long time ago, it has been mostly investigated on the macroscale, under uniform heating. Our approach is markedly different, since we are locally heating a microscale area, which implies a strong temperature gradient. The advantage is that the absence of nucleation centers (impurities, scratches, cavities, etc.) is much easier to ensure. Some works reported the generation of MBs when heating a microscale area using a resistively heated microwire. However, the presence of a microwire strongly affects the MB dynamics and morphology.<sup>33,34</sup>

In 2011, Hühn et al.<sup>20</sup> were the first to hypothesize that heating gold NP clusters in a liquid could lead to superheating due to the lack of nucleation centers. However, they refer to the presence of nucleation centers in the liquid itself, and not on the surface. In 2012, Carlson et al.<sup>35</sup> addressed the problem of superheating using the photothermal excitation of a single gold nanoparticle in water. They measure a boiling temperature of only  $T_{\text{B}} = 54$  °C, which is unexpectedly much lower than 100 °C. However, the authors argued that this value was underestimated due to the limited spatial resolution of their thermal imaging technique (the nanoparticle was around 400 nm in diameter and the distribution of the temperature not much larger than that in principle). In order to take into account this lack of resolution, the authors multiplied the measured temperature increase by a factor of 10.2, which led them to an estimation of the actual nanoparticle temperature of 320 °C, which turns out to be the spinodal decomposition of water. Our procedure and our conclusions are somehow different from the ones reported by Carlson et al. First, we do not suffer from a constraining spatial resolution, since we are heating micrometric areas and our spatial resolution is  $\sim 500$  nm.<sup>25</sup> The actual temperature is thus unambiguously the one we measure. Then, we never reached the spinodal temperature decomposition of water of 320 °C. We observe the formation of a bubble at a lower temperature, around 230 °C. Finally, we evidence that superheating in plasmonics does not require the heating of a single nanoparticle and can also be achieved over very large areas using assemblies of nanoparticles. In 2013, the Halas group studied experimentally and theoretically the formation of nano- and microbubbles generated around single spherical gold nanoparticles. They reported interesting features,

but they made the assumptions that the MBs were made of water steam and that a MB appears at 100 °C. Even though these assumptions seem intuitive at first sight, the underlying physics of the MB generation in plasmonics is more complex, as demonstrated by our experimental results.

Apart from these few recent developments in plasmonics, there is also a large community, specialized in fluid mechanics and phase transitions, which has been studying for long the physics of the generation of small bubbles. Below, we give a brief overview of the most important developments in this field, and explain how our contribution stands out from these developments.

A large community is working on the presence of *nanobubbles* at solid–liquid interfaces.<sup>36–38</sup> It has been observed using atomic force microscopes (AFMs) that nanobubbles were impinged in most liquid–solid interfaces and could exist for very long times (up to several days). These nanobubbles are too small to be observed by optical means. This is a quite peculiar and recent discovery that is still under investigation, since the origin and the nature of these nanobubbles are still not clearly explained. The bubbles considered in our experiments are completely different from these famous nanobubbles. They do not feature the same size, the same dynamics, and the same origin, since nanobubbles do not originate from heating.

Several studies have been reported on the physics of the micro- and nanobubble dynamics under cavitation.<sup>39–41</sup> This physics is quite different from the one related to our investigations. Indeed, cavitation is a bubble formation that results from a pressure decrease (not a temperature increase) which is usually very brief due to the propagation of a shock wave. Consequently, such bubbles are known to feature very short lifetimes and they are made of steam, not air (dissolved gas molecules do not have time to diffuse from the liquid environment to fill in the bubble).

Finally, another important area of research consists of the bubble generation under pulse heating.<sup>15,34,42</sup> The physics is also very different from what we report, as the bubbles collapse as fast as they appear (for the same reason as just above).

The context of our work is in that sense different and complementary in comparison with what was reported so far: the bubbles are observed on plasmonic structures, they are not nanometer sized, and they are generated under cw illumination.

**Bubble Shrinkage.** Once the MB is formed, if the heating beam is switched off, the temperature increase vanishes in a few microseconds due to the small size of the heated area. The time scale  $\tau$  of the cooling can be estimated using the relation  $\tau = L^2/D_T$ , where  $L$  is the characteristic size of the system and  $D_T$  its thermal diffusivity.<sup>13</sup> In our experiments,  $\tau$  is on the order of a fraction of a millisecond. However, the MB does not disappear straight away. It slowly shrinks during a few seconds, a few minutes, or even a few hours, depending on the initial size of the MB, before fully disappearing. The fact that the MB does not collapse as soon as the temperature increase vanishes stems from the nature of the MB: it is not made of steam water but of air molecules, as explained in the previous section. The air contained in the MB comes from the air molecules dissolved in the surrounding water. Under standard conditions, the molecular concentrations of O<sub>2</sub> and N<sub>2</sub> in water are, respectively, 0.26 and 0.50 mM, which corresponds approximately to 22 mL of air dissolved/L of water.

In order to investigate experimentally the MB dynamics, an area of approximately 7  $\mu\text{m}$  in diameter was heated above  $T_B$

during  $\Delta t = 20$  s to generate a MB in a steady state. Then, the heating (i.e., the laser) was stopped and a video was acquired at a rate of 25 frames per second to follow the MB diameter (see the video jp411519k\_si\_002.mov in the Supporting Information). The observations are reported in Figure 5 where the MB diameter is plotted as a function of time for four different MBs. The time origin was arbitrarily taken at the moment when the bubbles disappeared. The MB dynamics was observed to be fairly reproducible from one MB to another and a clear dependence of the bubble radius in  $(-t)^{1/3}$  is observed, regardless of the initial MB radius. In other words, the bubble lifetime  $\tau_{\text{MB}}$  is proportional to  $a^3$ , i.e., the volume of the bubble (Figure 5d). The measurements led to the fitting formula  $\tau_{\text{MB}} = 0.22a^3$  with  $\tau_{\text{MB}}$  in seconds and  $a$  in micrometers.

**Table 1. Notations Used in This Article**

name	description	dimension
$r$	radial coordinate	m
$t$	time	s
$a$	bubble radius	m
$V$	bubble volume	m <sup>3</sup>
$D$	laser beam diameter	m
$P_l$	laser power	W
$P$	bubble inner pressure	Pa
$P_\infty$	ambient pressure	Pa
$N$	amount of gas molecules in the bubble	mol
$T$	temperature	K
$Q$	absorbed power by NPs	W
$\Delta t$	heating duration	s
$c$	gas molecule concentration in the liquid	mol m <sup>-3</sup>
$c_\infty$	initial molecular concentration in the liquid	mol m <sup>-3</sup>
$J$	molecular flux density in the liquid	mol m <sup>-2</sup> s <sup>-1</sup>
$\gamma$	surface tension of the liquid/gas interface	J m <sup>-2</sup>
$K$	Henry coefficient	Pa m <sup>3</sup> mol <sup>-1</sup>
$D_T$	thermal diffusivity	m <sup>2</sup> s <sup>-1</sup>
$D$	molecular diffusivity	m <sup>2</sup> s <sup>-1</sup>
$D_s$	Soret coefficient	m <sup>2</sup> s <sup>-1</sup> K <sup>-1</sup>
$R$	gas constant	J mol <sup>-1</sup> K <sup>-1</sup>
$\kappa$	thermal conductivity	W m <sup>-1</sup> K <sup>-1</sup>

This simple  $a^3$  law stems from a subtle interplay between the Laplace pressure in the bubble and the molecular diffusion in the liquid. This law can be derived by assuming a spherical symmetry (discarding the substrate) where a gas MB stands in

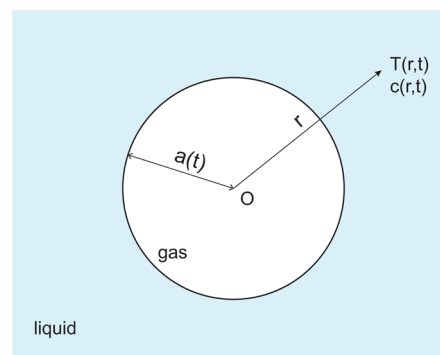


**Figure 4.** Schematic of the simplified system consisting of a gas bubble immersed in a uniform and isotropic liquid.

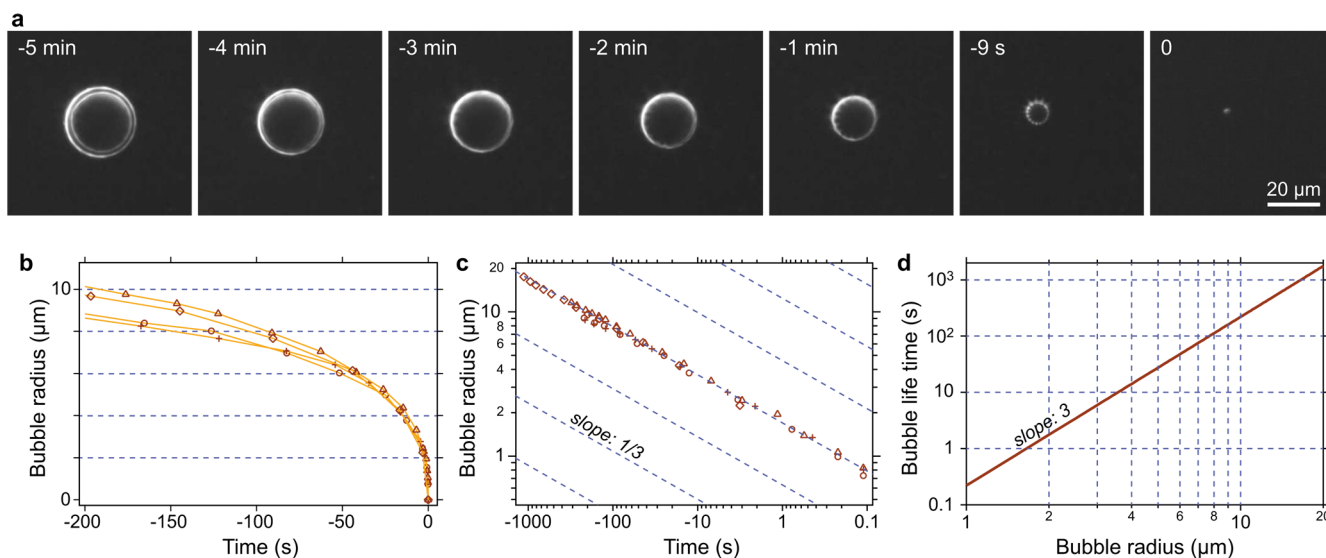


**Figure 5.** (a) Dark field images of a MB at successive times during shrinkage. (b) Evolution of the bubble radius  $a$  as a function of time for four different bubbles. The time origin is the bubble disappearance. (c) Same graph with a logarithmic scale. (d) MB lifetime as a function of the initial bubble radius (fit from experimental data).

a uniform and infinite liquid environment (Figure 4). The MB inner pressure as a function of the MB radius  $a$  reads

$$P = P_{\infty} + 2\gamma/a \quad (4)$$

where  $P_{\infty}$  is the ambient pressure and  $\gamma$  is the surface tension of the gas–liquid interface. If the gas is considered as ideal, it follows the ideal gas law  $PV = NRT$ , where  $V = 4\pi a^3/3$  is the MB volume,  $N$  is the amount of gas molecules (in moles),  $R$  is the gas constant, and  $T$  is the MB temperature. Using these two relations, one gets the constitutive equation relating the gas amount within the bubble and its radius:

$$N = \frac{4\pi a^3}{3RT} \left( P_{\infty} + \frac{2\gamma}{a} \right) \quad (5)$$

The molecule variation rate noted  $\dot{N} = dN/dt$  reads thus

$$\dot{N} = \frac{4\pi a^2 \dot{a}}{RT} \left( P_{\infty} + \frac{4\gamma}{3a} \right) \quad (6)$$

Let  $c(r, t)$  be the molar concentration of the gas dissolved in the liquid and constituting the MB.  $c$  is dependent on the radial coordinate  $r$  due to the central symmetry of the problem. The temporal variations of  $c$  are governed by a diffusion process (Fick's law) but also by the variation of the bubble size, which induces a centripetal overall fluid convection. The equation governing the gas concentration within the liquid is thus<sup>43</sup>

$$\partial_t c = \frac{D}{r^2} \partial_r (r^2 \partial_r c) + \frac{a^2 \dot{a}}{r^2} \partial_r c \quad (7)$$

On the right-hand side of eq 7, the first and second terms are, respectively, the diffusion and convection terms. In the context of this study, one can consider that the diffusion process is dominant, and neglect the contribution of the convective term. This assumption can be justified by dimensional analysis of the equation and based on the experimental observations: the order of magnitude of the ratio of the diffusive term by the convective term is on the order of  $D/(a\dot{a}) \gg 1$ . This amounts to making a quasistatic approximation where the variation of the bubble size is slow enough in comparison with the time scale of the molecular diffusion processes. Hence, if the convective term is

discarded in eq 7, one ends up with a regular diffusion equation and the solution simply reads

$$c(r, t) = c_{\infty} + \frac{c(a) - c_{\infty}}{r} a \quad (8)$$

The boundary condition  $c(a)$  is directly related to the inner bubble pressure  $P$  via the Henry law:

$$P = Kc(a) \quad (9)$$

Since  $P_{\infty} = Kc_{\infty}$  and using eqs 4 and 9, one gets

$$c(r, t) = c_{\infty} + \frac{2\gamma}{Kr} \quad (10)$$

Surprisingly, the molecular concentration in the liquid is not dependent on the size of the MB, i.e., not dependent on time. This means that, during the whole evolution of the MB radius, the concentration profile  $c(r, t)$  will not be affected. Hence, we can write  $c(r, t) = c(r)$ . Only its domain of definition  $[a(t), +\infty]$  will be time-dependent. The concentration profile is plotted in Figure 6a.

Let  $\mathbf{J}$  be the molecular flux density vector in the liquid.  $\mathbf{J}$  is radial, and its amplitude reads by definition

$$J(r) = -D\partial_r c(r) \quad (11)$$

$$J(r) = \frac{2\gamma D}{Kr^2} \quad (12)$$

By considerations on mass conservation, the molecular variation rate  $\dot{N}$  of the MB can be expressed as a function of  $J(a)$ :

$$\dot{N} = -4\pi a^2 J(a) \quad (13)$$

$$\dot{N} = -\frac{8\pi\gamma D}{K} \quad (14)$$

Interestingly, the delivering rate of gas molecules  $\dot{N}$  from the bubble to the surrounding liquid turns out to be constant during the bubble shrinkage. This is the origin of the fact that  $c(r)$  is constant, since  $c(r) = c_{\infty} + \dot{N}/(4\pi Dr)$ . From the two expressions of the molecule variation rates obtained in eqs 6

and 14, we finally obtain the differential equation governing the evolution of the MB radius:

$$\dot{a} = -\frac{2\gamma DRT}{Ka^2\left(P_\infty + \frac{4\gamma}{3a}\right)} \quad (15)$$

Two regimes can be expected depending on which term is dominant between  $P_\infty$  and  $\gamma/a$ . In water, the transition between these two regimes is obtained for  $a \approx 500$  nm. Since the purpose of this work is to investigate long-lived MBs that are at least a few micrometers in radius, we can discard the second term. Note that discarding this second term does not mean that the Laplace pressure does not play a role. Indeed,  $\gamma$  is still present in the simplified differential equation. In this approximation, the solution of eq 15 reads

$$a(t)^3 = -\frac{6RTD\gamma}{P_\infty K}t + \text{const} \quad (16)$$

From this equation, the lifetime of a MB can be simply estimated:

$$\tau_{\text{MB}} = \frac{P_\infty K}{6RTD\gamma}a^3 \quad (17)$$

The MB lifetime scales thus as  $a^3$ , i.e., the volume of the MB, as observed experimentally (see Figure 5d). Note that, in this model, the presence of the substrate is not taken into account. However, the presence of a surface is supposed to affect eq 13, since the MB surface will be smaller than  $4\pi a^2$ , and is supposed to affect eq 8 as well, since the surrounding medium no longer features a central symmetry. Taking these corrections into account would add a correction factor to the estimated lifetime but would not change the power-three dependence.

#### Bubble Steady State Maintained under Illumination.

We have investigated in the previous sections the physics of the formation of a MB under illumination and of the shrinkage of the MB upon stopping the illumination. In this section, we shall describe the bubble *steady state* under illumination.

In the following, we consider that the laser beam diameter is smaller than the bubble diameter ( $D < 2a$ ), so that the heat power  $Q$  is generated inside the MB. This assumption simplifies the discussion, and matches what was done experimentally. As the heating laser is on, a temperature gradient is expected within the medium. Since the temperature profile is no longer uniform in the system, the new molecular flux density vector now reads<sup>44</sup>

$$\mathbf{J} = -D\nabla c - D_s c \nabla T \quad (18)$$

The second contribution involving the temperature gradient expresses thermophoresis. Thermophoresis is a process that induces a diffusion of dissolved species in a liquid due to a temperature gradient.<sup>44</sup> Most of the time, dissolved species tend to move toward colder regions ( $D_s > 0$ ). As we consider a steady state,  $\dot{c} = -\nabla \cdot \mathbf{J} = 0$ , which yields

$$\nabla \cdot (-D\nabla c) = \nabla \cdot (D_s c \nabla T) \quad (19)$$

$$-D\nabla^2 c = D_s c \nabla^2 T + D_s \nabla c \cdot \nabla T \quad (20)$$

As the steady state temperature profile is governed by the Laplace equation,  $\nabla^2 T = 0$  and  $T(r) = Q/(4\pi\kappa r)$ , where  $\kappa$  is the thermal conductivity of the liquid. Using this expression in eq 20 leads to the differential equation governing the molecular concentration around the MB, under illumination:

$$\frac{1}{r} \partial_r [r \partial_r c(r)] = \frac{D_s}{D} \frac{Q}{4\pi\kappa r^2} \partial_r c(r) \quad (21)$$

The solution of this equation fulfilling the boundary conditions  $\lim_{r \rightarrow \infty} c(r) = c_\infty$  and  $\lim_{r \rightarrow \infty} \partial_r c(r) = 0$  is

$$c(r) = c_\infty \exp\left(-\frac{D_s Q}{D 4\pi\kappa r}\right) \equiv c_\infty e^{-r_d/r} \quad (22)$$

where

$$r_d = \frac{D_s Q}{D 4\pi\kappa} \quad (23)$$

is the depletion length of the molecular concentration around the MB induced by thermophoresis.

As a conclusion, during heating, the steady state is characterized by a molecule depletion at the vicinity of the MB. On the contrary, upon stopping heating (during the bubble shrinkage), the opposite effect occurs: a molecule accumulation is observed around the MB (see previous section). This is summarized in Figure 6.

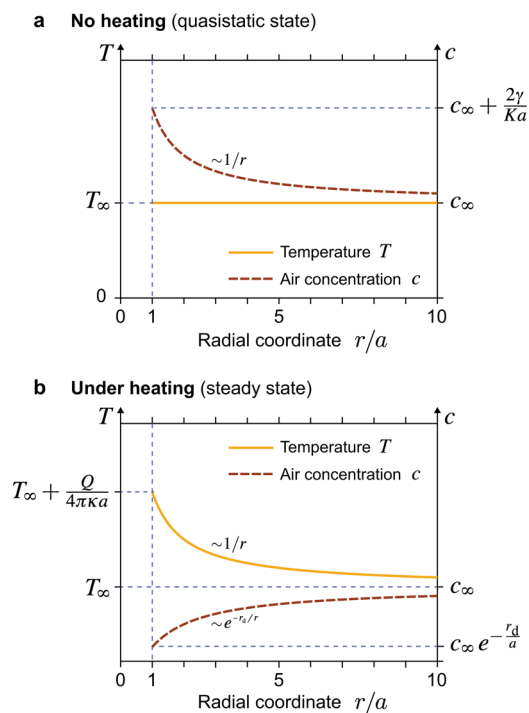


**Figure 6.** (a) Radial temperature profile in the liquid surrounding a MB of radius  $a$ , both under heating and without heating. (b) Associated radial profile of the molecular concentration of the gas dissolved in the surrounding medium (plotted for the particular case of  $r_d = a$ ).

Let us now discuss a singular observation that often occurs when illuminating a MB on plasmonic nanoparticles. In our experiments, in order to maintain the bubble under a steady state, the laser beam was focused on gold nanoparticles located around the center of the MB (Figure 1b). These heated nanoparticles were thus no longer surrounded by water but by a gas phase. If this focused heating beam is moved toward the edge of the MB, at the glass/water/gas junction (see Figure 7e) or even a few micrometers away from the MB, it is possible to induce boiling within the MB, without affecting the MB itself. Successive images of a MB boiling event are displayed in Figure

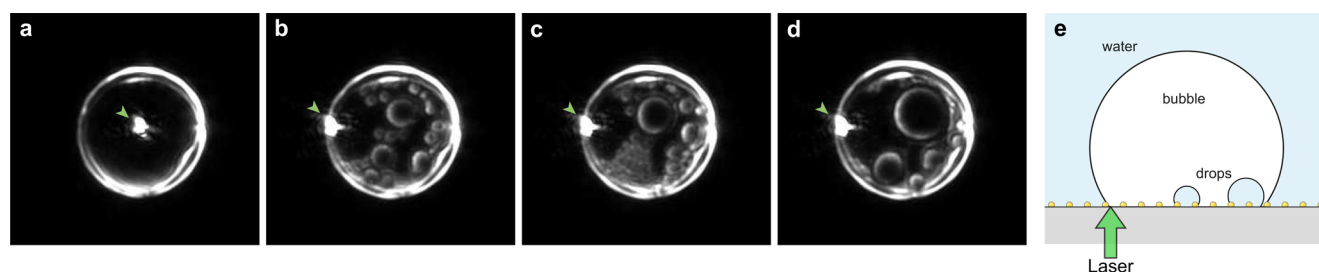


**Figure 7.** Successive dark field images of a single MB (see the video jp411519k\_si\_002.mov in the Supporting Information). (a) Initial MB with the heating focused in the center of the bubble. (b–d) Successive images when the laser is focused near the water–bubble interface, evidencing boiling inside the bubble. (e) Schematic side view of the system.

7a–d. Boiling is induced at the edge of the MB, which produces a large amount of steam within the MB, which recondenses instantaneously nearby the other extremity of the MB, where the temperature of the substrate is lower and below 100 °C. This is the origin of the observation of water microdrops within the bubble. When the heating is stopped, these water microdrops within the MB are stable. However, if the laser beam is focused right within the MB, they all evaporate instantaneously. A video evidencing these phenomena is provided in the Supporting Information (jp411519k\_si\_003.mov).

This observation illustrates that complex and unexpected processes may occur when investigating phase transitions and fluid dynamics on the microscale.<sup>45</sup> For this purpose, plasmonic nanoparticles, and especially gold nanoparticles, are good candidates for several reasons: they lead to large optical absorption with a low quantity of metal, they are biocompatible, they do not suffer from oxidation, and they feature catalytic properties, which could lead to new applications in solvothermal chemistry.<sup>46,47</sup> Solvothermal (respectively hydrothermal) chemistry is a branch of chemistry based on the use of superheated liquids (respectively water) as solvents. For this purpose, the use of a pressured chamber (autoclave) is necessary to avoid boiling. Our approach based on the use of plasmonic NPs would not require the use of an autoclave, which could certainly open the path for new synthetic experimental procedures in chemistry.

## CONCLUSION

To summarize, we first focused on the physics of the generation of microbubbles. We explained that no microbubble is expected at 100 °C for two reasons: a too small bubble curvature radius that increases the boiling point and the absence of nucleation centers in our samples. Supercritical liquid water, up to 220 °C, are systematically observed prior to bubble formation, regardless of the size of the heated area. Then, we described the physics of the bubble shrinkage once the heating is turned off. We evidenced experimentally very long lifetimes, due to the fact that the MBs are not made of water steam but of air molecules coming from the liquid. The lifetime is proportional to the MB volume and can reach several tens of minutes. A theory is developed to explain this feature, and we evidenced that the dynamics is governed by a diffusion process of the gas molecules in the liquid.

All this work strongly benefits from the capabilities of our TIQSI thermal imaging technique that we recently developed.<sup>25</sup> Indeed, this microscopy technique makes it possible to measure temperature over a wide range of values, with no real upper limitation, mainly because our technique is label free, and not

based on the use of temperature-sensitive fluorescent molecules likely to thermobleach around 70 °C.<sup>48</sup>

All of these observations evidence how interesting and complex a thermal-induced fluid mechanism can be on the microscale, especially when phase transitions are involved. We hope that this work will be the basis for new fundamental investigations in fluid mechanics and phase transition on the microscale. We also foresee valuable applications especially in chemistry: the ability of heating a fluid far above 100 °C without using an autoclave would certainly open the path for new synthetic pathways in chemistry. Moreover, gold nanoparticles are known to feature catalytic properties for some chemical reactions, especially at high temperatures, which appears to be another promising benefit of such an approach.

## ASSOCIATED CONTENT

### Supporting Information

Details of the sample geometry and of the refractive index variation as a function of temperature. jp411519k\_si\_002.mov: Shrinkage of a microbubble. jp411519k\_si\_003.mov: Internal boiling. This material is available free of charge via the Internet at <http://pubs.acs.org>.

## AUTHOR INFORMATION

### Corresponding Author

\*E-mail: [guillaume.baffou@Fresnel.fr](mailto:guillaume.baffou@Fresnel.fr). Phone: +33(0) 491288495.

### Notes

The authors declare no competing financial interest.

## ACKNOWLEDGMENTS

We thank Marc Médale and Nora Chérifa Abid from the IUSTI, Marseille, France, for helpful discussions and acknowledge financial support from the Deutsche Forschungsgemeinschaft (DFG) and the Max Planck Society.

## REFERENCES

- Baffou, G.; Quidant, R. Thermo-plasmonics: Using Metallic Nanostructures as Nano-Sources of Heat. *Laser Photonics Rev.* **2013**, *7*, 171–187.
- Lal, S.; Clare, S. E.; Halas, N. J. Nanoshell-Enabled Photothermal Cancer Therapy: Impending Clinical Impact. *Acc. Chem. Res.* **2008**, *41*, 1842.
- Cognet, L.; Berciaud, S.; Lasne, D.; Lounis, B. Photothermal Methods for Single Nonluminescent Nano-Objects. *Anal. Chem.* **2008**, *80*, 2288–2294.
- Ghosh, P.; Han, G.; De, M.; Kim, C. K.; Rotello, V. M. Gold Nanoparticles in Delivery Applications. *Adv. Drug Delivery Rev.* **2008**, *60*, 1307–1315.

- (5) Delcea, M.; Sternberg, N.; Yashchenok, A. M.; Georgieva, R.; Bäuml, H.; Möhwald, H.; Skirtach, A. G. Nanoplasmonics for Dual-Molecule Release through Nanopores in the Membrane of Red Blood Cells. *ACS Nano* **2012**, *6*, 4169–4180.
- (6) Eghtedari, M.; Oraevsky, A.; Copland, J.; Kotov, N.; Conjusteau, A.; Motamedi, M. High intensity of *in vivo* detection of gold nanorods using a laser optoacoustic imaging system. *Nano Lett.* **2007**, *7*, 1914–1918.
- (7) Kim, C.; Cho, E. C.; Chen, J.; Song, K. H.; Au, L.; Favazza, C.; Zhang, Q.; Cobley, C. M.; Gao, F.; Xia, Y.; et al. *In vivo* molecular photoacoustic tomography of melanomas targeted by bioconjugated gold nanocages. *ACS Nano* **2010**, *4*, 4559–4564.
- (8) Xiao, M.; Jiang, R.; Wang, F.; Fang, C.; Wang, J. Plasmon-enhanced chemical reactions. *J. Mater. Chem. A* **2013**, *1*, 5790–5805.
- (9) Zhu, M.; Baffou, G.; Meyerbröker, N.; Polleux, J. Micropatterning Thermoplasmonics Gold Nanoarrays to Manipulate Cell Adhesion. *ACS Nano* **2012**, *6*, 7227–7233.
- (10) Zhao, C.; Liu, Y.; Zhao, Y.; Fang, N.; Huang, T. J. A Reconfigurable Plasmo-fluidic Lens. *Nat. Commun.* **2013**, *4*, 2305.
- (11) Kim, J. Joining Plasmonics with Microfluidics: From Convenience to Inevitability. *Lab Chip* **2012**, *12*, 3611–3623.
- (12) Donner, J.; Baffou, G.; McCloskey, D.; Quidant, R. Plasmon-Assisted Optofluidics. *ACS Nano* **2011**, *5*, 5457–5462.
- (13) Baffou, G.; Rigneault, H. Femtosecond-Pulsed Optical Heating of Gold Nanoparticles. *Phys. Rev. B* **2011**, *84*, 035415.
- (14) Lukianova-Hleb, E.; Hu, Y.; Latterini, L.; Tarpani, L.; Lee, S.; Drezek, R. A.; Hafner, J. H.; Lapotko, D. O. Plasmonic Nanobubbles as Transient Vapor Nanobubbles Generated around Plasmonic Nanoparticles. *ACS Nano* **2010**, *4*, 2109.
- (15) Kotaidis, V.; Dahmen, C.; von Plessen, G.; Springer, F.; Plech, A. Excitation of nanoscale vapor bubbles at the surface of gold nanoparticles in water. *J. Chem. Phys.* **2006**, *124*, 184702.
- (16) Kotaidis, V.; Plech, A. Cavitation on the nanoscale. *Appl. Phys. Lett.* **2005**, *87*, 213102.
- (17) Lukianova-Hleb, E. Y.; Koneva, I. I.; Oginsky, A. O.; La Francesca, S.; Lapotko, D. O. Selective and Self-Guided Micro-Ablation of Tissue with Plasmonic Nanobubbles. *J. Surg. Res.* **2011**, *166*, e3–e13.
- (18) Vogel, A.; Venugopalan, V. Mechanisms of pulsed laser ablation of biological tissues. *Chem. Rev.* **2003**, *103*, 577.
- (19) Brujan, E. A.; Vogel, A. Stress wave emission and cavitation bubble dynamics by nanosecond optical breakdown in a tissue phantom. *J. Fluid Mech.* **2006**, *558*, 281–308.
- (20) Hühn, D.; Govorov, A.; Rivera Gil, P.; Parak, W. J. Biological media: Characterization of mechanical destruction and boiling. *Adv. Funct. Mater.* **2012**, *22*, 294–303.
- (21) Neumann, O.; Urban, A. S.; Day, J.; Lal, S.; Nordlander, P.; Halas, N. J. Solar Vapor Generation enabled by nanoparticles. *ACS Nano* **2013**, *7*, 42–49.
- (22) Fang, Z.; Zhen, Y. R.; Neumann, O.; Polman, A.; García de Abajo, F. J.; Nordlander, P.; Halas, N. J. Evolution of Light-Induced Vapor Generation at a Liquid-Immersed Metallic Nanoparticle. *Nano Lett.* **2013**, *13*, 1736–1742.
- (23) Polleux, J.; Rasp, M.; Louban, I.; Plath, N.; Feldhoff, A.; Spatz, J. P. Benzyl Alcohol and Block Copolymer Micellar Lithography: A Versatile Route to Assembling Gold and *In Situ* Generated Titania Nanoparticles into Uniform Binary Nanoarrays. *ACS Nano* **2011**, *5*, 6355–6364.
- (24) Baffou, G.; Berto, P.; Bermúdez Ureña, E.; Quidant, R.; Monneret, S.; Polleux, J.; Rigneault, H. Photoinduced Heating of Nanoparticle Arrays. *ACS Nano* **2013**, *7*, 6478–6488.
- (25) Baffou, G.; Bon, P.; Savatier, J.; Polleux, J.; Zhu, M.; Merlin, M.; Rigneault, H.; Monneret, S. Thermal Imaging of Nanostructures by Quantitative Optical Phase Analysis. *ACS Nano* **2012**, *6*, 2452–2458.
- (26) Purchased from Phasics SA, Palaiseau, France; www.phasicscorp.com.
- (27) Schiebener, P.; Straub, J.; Levelt Sengers, J. M. H.; Gallagher, J. S. Refractive Index of Water and Steam as Function of Wavelength, Temperature and Density. *J. Phys. Chem. Ref. Data* **1990**, *19*, 677.
- (28) Bon, P.; Belaid, N.; Lagrange, D.; Bergaud, C.; Rigneault, H.; Monneret, S.; Baffou, G. Three-dimensional temperature imaging around a gold microwire. *Appl. Phys. Lett.* **2013**, *102*, 244103.
- (29) Dammer, S. M.; Lohse, D. Gas Enrichment at Liquid-Wall Interfaces. *Phys. Rev. Lett.* **2006**, *96*, 206101.
- (30) Belova, V.; Krasowska, M.; Wang, D.; Ralston, J.; Shchukin, D. G.; Möhwald, H. Influence of adsorbed gas at liquid/solid interfaces on heterogeneous cavitation. *Chem. Sci.* **2013**, *4*, 248.
- (31) Deguchi, S.; Takahashi, S.; Hiraki, H.; Tanimura, S. Direct measurement of force exerted during single microbubble generation. *Appl. Phys. Lett.* **2013**, *102*, 084101.
- (32) Caupin, F.; Herbert, E. Cavitation in Water: A Review. *C. R. Physique* **2006**, *7*, 1000–1017.
- (33) Glod, S.; Poulidakos, D.; Zhao, Z.; Yadigaroglu, G. An investigation of microscale explosive vaporization of water on an ultrathin Pt wire. *Int. J. Heat Mass Transfer* **2002**, *45*, 367–379.
- (34) Deng, P. D.; Lee, Y. K.; Cheng, P. An experimental study of heater size effect on micro bubble generation. *Int. J. Heat Mass Transfer* **2006**, *49*, 2535.
- (35) Carlson, M. T.; Green, A. J.; Richardson, H. H. Superheating Water by CW Excitation of Gold Nanodots. *Nano Lett.* **2012**, *12*, 1534.
- (36) Craig, V. S. J. Very Small Bubbles at Surfaces – the nanobubble puzzle. *Soft Matter* **2011**, *7*, 40.
- (37) Ball, P. Nanobubbles are not Superficial Matter. *ChemPhysChem* **2012**, *13*, 2173–2177.
- (38) Weijs, J. H.; Lohse, D. Why Surface Nanobubbles Live for Hours. *Phys. Rev. Lett.* **2013**, *110*, 054501.
- (39) Plesset, M. S. Bubble dynamics and cavitation. *Annu. Rev. Fluid Mech.* **1977**, *9*, 145–185.
- (40) Lugli, F.; Zerbetto, F. An introduction to bubble dynamics. *Phys. Chem. Chem. Phys.* **2007**, *9*, 2447–2456.
- (41) Brujan, E. A. Numerical investigation on the dynamics of cavitation nanobubbles. *Microfluid. Nanofluid.* **2011**, *11*, 511–517.
- (42) Deng, P.; Lee, Y. K.; Cheng, P. The growth and collapse of a micro-bubble under pulse heating. *Int. J. Heat Mass Transfer* **2003**, *46*, 4041–4050.
- (43) Ljunggren, S.; Eriksson, J. C. The lifetime of a colloid-sized gas bubble in water and the cause of the hydrophobic attraction. *Colloids Surf., A* **1997**, *129–130*, 151–155.
- (44) Duhr, S.; Braun, D. Why molecules move along a temperature gradient. *Proc. Natl. Acad. Sci. U.S.A.* **2006**, *103*, 19678.
- (45) Govorov, A. O.; Zhang, W.; Skeini, T.; Richardson, H.; Lee, J.; Kotov, N. A. Gold Nanoparticle Ensembles as Heaters and Actuators: Melting and Collective Plasmon Resonances. *Nanoscale Res. Lett.* **2006**, *1*, 84.
- (46) Savage, P. E. Organic Chemical Reactions in Supercritical Water. *Chem. Rev.* **1999**, *99*, 603–621.
- (47) Savage, P. E. Heterogeneous Catalysis in Supercritical Water. *Catal. Today* **2000**, *62*, 167–173.
- (48) Baffou, G.; Kreuzer, M. P.; Kulzer, F.; Quidant, R. Temperature mapping near plasmonic nanostructures using fluorescence polarization anisotropy. *Opt. Express* **2009**, *17*, 3291.